Optimization of a magnetostatic cavity for a ^{3}He spin analyzer on the CANDOR polychromatic reflectometer

Journal of Physics: Conference Series **1316** (2019) 012017 doi:10.1088/1742-6596/1316/1/012017

Optimization of a magnetostatic cavity for a ^{3}He spin analyzer on the CANDOR polychromatic reflectometer

Md. T. Hassan[1,2], **W.C. Chen**[1,2,*]

[1] National Institute of Standards and Technology, Gaithersburg, Maryland 20899, USA
[2] University of Maryland, College Park, Maryland 20742, USA

E-mail: wcchen@nist.gov

Abstract.

A new instrument, the CANDOR (Chromatic Analysis Neutron Diffractometer or Reflectometer) polychromatic beam reflectometer is being built at the National Institute of Standards and Technology Center for Neutron Research. CANDOR will have a capability of polarization analysis for both specular and off-specular scattering, and allow for measuring the magnetic structures of magnetic thin films with a significantly shortened measurement time as compared to a conventional monochromatic beam reflectometer at a continuous neutron source. A critical component of the polarization analysis capability is to develop a ^{3}He neutron spin filter (NSF) for polarization analysis for both specular and off-specular scattering for a continuous wavelength range between 4 Å and 6 Å and a large solid angle coverage for up to 20 energy dispersive detector channels. For *ex-situ* spin-exchange optical pumping (SEOP) operation, a magnetically shielded solenoid (MSS) will be employed to provide a volume averaged field gradient, $|\vec{\nabla}B_\perp/B|$, better than 5×10^{-4} cm^{-1} to maintain ^{3}He polarization relaxation times of at least a few hundred hours on the beam line even when there are significant stray fields from a magnet operating at a field up to 3 T at the sample position. We describe a procedure to design, construct, and optimize a MSS with non-identical compensation coil dimensions on the ends to match the scattered neutron beam rays. The volume averaged field gradient is quantified and optimized over a cell for a MSS using the finite-element software package RADIA and compared with that from the experiment.

Key words: polychromatic reflectometer, CANDOR, SEOP, ^{3}He neutron spin filter, field gradient

1. Introduction

A conventional monochromatic reflectometer at a continuous source utilizes either a pyrolytic graphite (PG) crystal or a velocity selector to monochromatize the incident beam and detects neutrons elastically scattered from the sample without energy analysis. At the National Institute of Standards and Technology (NIST) Center for Neutron Research a novel instrument, the CANDOR (Chromatic Analysis Neutron Diffractometer or Reflectometer) polychromatic beam reflectometer is being built and is expected to be commissioned soon. CANDOR utilizes a polychromatic beam with incident neutron wavelengths (energies) between 4 Å (5.113 meV) and 6 Å (2.272 meV) that are closely matched to the peak flux of the neutron spectra from the NCNR's cold neutron source [1]. The energy determination is accomplished at the scattered

beam side using a linear array of PG crystals, similar to the Continuous Angle Multiple Energy Analysis (CAMEA) concept of the multi-analyzer module MultiFlexx of the cold triple axis spectrometer FLEXX [2]. The analyzer system employs a bank of 18 energy dispersive detector channels, each covering an angular range of 0.355 °, each containing 54 graphite analyzer crystals in series with corresponding scintillation detector plates. The total angular coverage for the scattered beam will be 6.4 °. The neutron detection system after the PG crystals is one of the most critical units for the CANDOR development and has been accomplished using a slab of LiF:ZnS(Ag) scintillator with embedded wavelength shifting fibers and a silicon photomultiplier used as a photosensor [3]. It is expected that CANDOR will provide significantly higher usable intensity incident on sample, hence reducing measurement times significantly for a given sample size over a conventional continuous source-based monochromatic reflectometer.

CANDOR will be equipped with a longitudinal polarization analysis capability for both specular and off-specular reflectivity measurements. For the polarized beam configuration, a double-V supermirror made by SwissNeutronics [4] is used to polarize the incident neutron beam and is expected to provide a neutron polarization of 98 % or higher for the entire wavelength range from 4 Å to 6 Å. An adiabatic radio-frequency (RF) spin flipper located immediately following the monochromator is used to flip the neutron spin over a large cross sectional beam with a flipping efficiency better than 99.5 % [5]. To spin analyze the neutron polarization of the scattered beam, it is necessary to have a spin analyzer able to cover the entire 6.4 ° angular range for the entire energy range and provide a spatially uniform analyzing power higher than 98 %, and have a second broadband spin flipper with a flipping efficiency higher than 99.5 % over a large cross sectional scattered neutron beam. Given the space of 60 cm available for both the spin analyzer and the broadband spin flipper, a ^{3}He neutron spin filter (NSF) was chosen for the following reasons. A ^{3}He NSF can (1) polarize a broad wavelength band of neutrons effectively; (2) polarize large area and widely divergent neutron beams; and (3) efficiently flip the neutron polarization by reversing the ^{3}He nuclear polarization using the adiabatic fast passage (AFP) nuclear magnetic resonance (NMR) technique [6], hence integrating the analyzer and flipper into a single device. The advantage of integration of the analyzer and the broadband flipper into a single neutron polarizing device is a unique feature of the ^{3}He analyzer since no other conventional neutron spin analyzer and flipper together can be fit into a 60-cm space along the beam path for the CANDOR scattered beam configuration. At the NCNR, ^{3}He NSFs have been routinely applied to small-angle neutron scattering, triple-axis spectrometry, and wide-angle polarization analysis [7]. A ^{3}He NSF has been demonstrated previously for polarization analysis of the diffusely reflected neutrons on the polarized neutron reflectometer at the NCNR [8, 9].

For ^{3}He NSF applications in polarized neutron scattering, a cylindrical geometric shape is generally chosen for a ^{3}He cell. For the CANDOR analyzer, a cylindrical ^{3}He cell with a diameter of 13 cm or larger is necessary for covering the scattering angle subtended by the entire detector bank. For this large ^{3}He cell, we plan to operate the ^{3}He NSF in the *ex-situ* spin exchange optical pumping (SEOP) operation mode. The ^{3}He gas is polarized in sealed cells in an off-line lab using the SEOP method, and the cells are transported to the beam line in a portable solenoid. In the *ex-situ* SEOP operation mode, it is critical to maintain the relaxation time of nuclear-polarized ^{3}He gas as long as possible. The relaxation time T_1 of the polarized ^{3}He gas has three contributions 1) dipole-dipole interactions [10], T_1^{dd}, 2) wall relaxation [11], T_1^{w}, 3) magnetic field gradients [12], T_1^{fg}, and is given by

$$\frac{1}{T_1} = \frac{1}{T_1^{\mathrm{dd}}} + \frac{1}{T_1^{\mathrm{w}}} + \frac{1}{T_1^{\mathrm{fg}}} \tag{1}$$

The dipole-dipole relaxation rate increases linearly with the partial pressure of ^{3}He gas and has been determined to be $p/807$ (h^{-1}) for p in bar [10]. The relaxation rate due to magnetic-field gradients is directly proportional to the square of the fractional transverse field gradients and

inversely proportional to the ^{3}He pressure [12]. As discussed in Eq. 2 later, for a cell at a pressure of one bar in a uniform gradient of $|\vec{\nabla}B_\perp/B|$=5 $\times$ 10^{-4} cm^{-1} the gradient-induced relaxation time is ≈600 h. For a given ^{3}He polarization of 85 %, which can be routinely achieved at NIST with the SEOP method using the spectrally narrowed high power diode bar lasers [13], it is desired to have a ^{3}He partial pressure of ≈1 bar for the CANDOR ^{3}He analyzer for optimizing the analyzing power and transmission. This implies a dipole-dipole relaxation time of ≈800 h. The current best ^{3}He cell fabrication practice has nearly eliminated the wall relaxation rate (with the wall relaxation time longer than 3000 h) in certain ^{3}He cells [14, 15]. Specifically we have successfully developed ^{3}He cells for CANDOR with relaxation times between 450 h and 690 h, measured under a homogeneous magnetic field with the field gradient $|\vec{\nabla}B_\perp/B|$ better than 1×10^{-4} cm^{-1}. For the best cell, this implies a wall relaxation time longer than 5000 h. In order to achieve a relaxation time of 250 h or longer for the ^{3}He analyzer, a volume averaged field gradient upper limit of 5×10^{-4} cm^{-1} is required.

The polarization analysis capability on CANDOR will likely use a hybrid 3 T superconducting magnet at the sample with the field along the vertical direction. In order to effectively shield stray fields from the 3 T magnet, we will employ a magnetically shielded solenoid (MSS) to maintain the ^{3}He polarization on the CANDOR beam line. Several different magnetically shielded solenoids have been developed to maintain the ^{3}He polarization for several polarized beam instruments at the NCNR, and are able to shield stray fields of approximately a few mT, produced from either an electromagnet or even a superconducting magnet [7]. Furthermore, it is necessary to implement a neutron spin rotation device to adiabatically rotate the spin from the vertical to longitudinal direction. Under such an operating configuration, it is still necessary to maintain volume average field gradient better than 5×10^{-4} cm^{-1}. In this paper we describe modeling of the field gradients, design and construction of the CANDOR MSS, and characterization of field gradients for the ^{3}He spin analyzer on CANDOR.

2. Modeling

Similar to our previous designs of solenoids [7, 9, 16, 17, 18], the 16 AWG (American Wire Gauge) 1.31 mm diameter copper wire was wound on an aluminum cylinder which was nested inside a Conetic mu-metal [19] cylinder. The gap between the two cylinders is typically 7 mm. On each end of the mu-metal solenoid, a Conetic mu-metal end cap is tightly attached to the mu-metal cylinder body with an overlap of 2.5 cm. The overlap protects the mu-metal from saturation even when applying a modest current to the aluminum solenoid. A hole in each end cap lets neutrons pass through without neutron depolarization. Fig. 1 shows a schematic of the CANDOR MSS. Notable features in Fig. 1 include a RF coil structure that is used to invert the ^{3}He polarization, compensation coils centered to each end cap hole, and borated aluminum neutron shields attached to both the upstream end cap and the downstream compensation coil frame. We began by determining the dimensions of the CANDOR MSS with the aim of designing the solenoid to be as compact as possible, while still achieving a volume averaged field gradient better than 5×10^{-4} cm^{-1}. Based on the ^{3}He cell diameter requirement, we determined the diameters of the aluminum cylinder and mu-metal cylinder to be 261 mm and 279 mm, respectively. The length of the mu-metal solenoid was determined to be 356 mm by taking the following facts into consideration: (1) the total space available, (2) the space necessary for a device to accomplish an adiabatic $\pi/2$ spin rotation, (3) the effect of the magnetic field from the adiabatic spin rotation device on the field gradient of the MSS. Unlike magnetically shielded solenoids developed earlier at the NCNR [7] where the same number of ampere-turns in two identical compensation coils have been used, we used compensation coils with different diameters and hence different number of ampere-turns in order to further improve the field gradient and/or make it more compact for the CANDOR MSS. The diameters for the compensation coils were determined to be 117 mm and 143 mm attached to the upstream and

downstream end caps, respectively. The compensation coils were wound on a 5.8 mm wide and 4 mm deep aluminum groove structure that was attached to the mu-metal end cap as shown in Fig. 1. The groove structure displaced the compensation coils by 3 mm along z and 2.8 mm in the radial direction from the end cap hole. As discussed later, the field gradient induced relaxation rate with non-identical compensation coils will be reduced by a factor of 1.88 over the conventional identical compensation coils. An additional benefit of using non-identical compensation coils is a possibility of reducing the diameter of the ^{3}He analyzer cell since the field homogeneity center is shifted closer to the upstream end cap as described later.

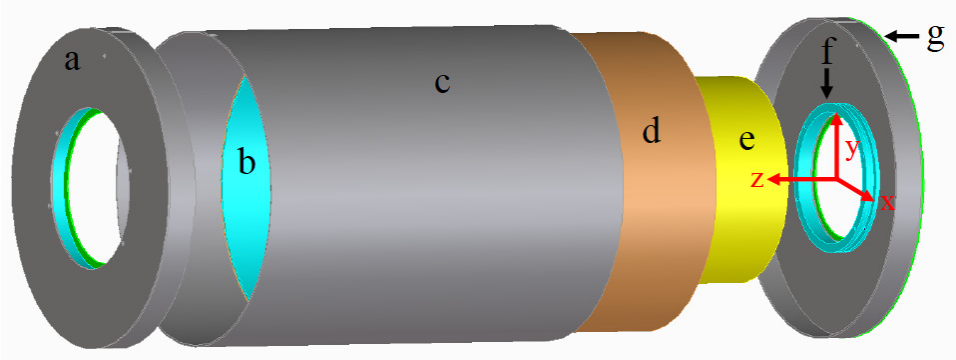

Figure 1. (Color online) Schematic of a magnetically shielded solenoid with circular holes in the end caps. The MSS is 279 mm in diameter, 356 mm long, with different sizes (117 mm diameter and 143 mm diameter) of holes on the end caps as described in the text. The MSS has the following components, (a) Conetic [19] mu-metal end caps, (b) aluminum cylinder with a wall thickness of 2.4 mm for support of the copper winding, (c) Conetic [19] mu-metal cylinder, (d) copper winding, (e) RF coil structure, (f) compensation coils centered to the end cap hole, (g) borated aluminum neutron shielding piece attached to the end cap in the upstream direction. The thickness for all mu-metal pieces is 1.6 mm.

We proceed to discuss the simulation of the magnetic field profile, the resulting field gradients, and optimization of compensation coils of the CANDOR MSS. A similar simulation and modeling has been completely described for our earlier development of a compact end-compensated magic box [20]. The field gradients relevant to the relaxation of polarized ^{3}He gas are $\vec{\nabla}B_x$ and $\vec{\nabla}B_y$, using the coordinate system in Fig. 1. These six gradients of field components, all perpendicular to the applied field, contribute over the volume, V, of a cell to the relaxation time of the polarized ^{3}He gas. At room temperature, the relaxation rate $1/T_1^{\rm fg}$ due to field gradients is given by

$$\frac{1}{T_1^{\rm fg}} = \frac{6700}{pV}\iiint_V \left(\frac{|\,\vec{\nabla}B_x\,|^2}{B^2} + \frac{|\,\vec{\nabla}B_y\,|^2}{B^2}\right) dx\,dy\,dz \;\; {\rm h}^{-1} \equiv \frac{6700}{p}|\vec{\nabla}B_\perp/B|^2 \;\; {\rm h}^{-1} \qquad (2)$$

where p is the gas pressure in bar and $\frac{\vec{\nabla}B_x}{B}$ and $\frac{\vec{\nabla}B_y}{B}$ are the gradients in the transverse components of the magnetic field (for nuclear polarization along the z-axis) normalized to the central field, B, in units of cm^{-1}[21]. $|\vec{\nabla}B_\perp/B|$ is the normalized volume-averaged transverse gradient over the cell volume, V. In practice, these transverse components are too tiny ($< 0.1\mu$T) to measure experimentally for a field gradient level of 10^{-4} cm^{-1} using conventional means. As demonstrated in an earlier publication [20], the conveniently measurable gradient component along the applied field $|\partial B_z/\partial z|/B$ was a good indicator of the normalized volume-averaged transverse field gradient.

We used the finite-element software package RADIA [22] for the field profile and the Mathematica [23] interface for analytical calculation of the magnetic field gradients. We modeled and optimized the CANDOR MSS with three different configurations: (i) the upstream compensation coil with an inner diameter of 117 mm and downstream compensation coil with an inner diameter of 143 mm, both upstream and downstream compensation coils with a diameter of 117 mm (ii) and 143 mm (iii). The criterion for convergence of the RADIA simulation iterations was that the magnetization of all segments changed by less than 10 nT. The segment size was determined to be about 4.6 mm (78 sections) along z and 6.67 ° (54 sections) radially in the x-y plane by confirming the normalized volume-averaged field gradients changed by less than 10^{-5} cm^{-1}.

We began to model the MSS with two identical compensation coils with an inner diameter of 117 mm and 143 cm as it is more straightforward and has been done for earlier development of the MSSs [7]. For the simulations, no air gap was used between the mu-metal cylinder body and each end cap in the 2.5 cm overlap section. The main coil winding section on the aluminum cylinder was extended to be in contact with each mu-metal cap. The compensation coil winding was fixed at 3 layers and 4.5 turns per layer in the groove. Changing the compensation coil was done via a change of the current dennsity. This closely matched to the experimentally field mapped condition since varying the number of the compensation coils was impractical during mapping. Other geometric dimensions for the simulation are identical to that from Fig. 1. The field in the center of the solenoid was fixed at about 2.73 mT. We found that at the optimized conditions the number of the compensation coils were 12 turns and 16 turns, corresponding to a ratio of ampere-turn of 0.044 and 0.059 between the compensation coil of an inner diameter of 117 mm and the main coil, and between the compensation coil of an inner diameter of 143 mm and the main coil, respectively. The volume averaged gradients $|\vec{\nabla}B_{\perp}/B|$ were calculated over a cylindrical ^{3}He cell, 120 mm in diameter and 100 mm long with a cylindrical axis along z. These gradients were determined to be 2.6×10^{-4} cm^{-1} and 4.8×10^{-4} cm^{-1}, for compensation coils of inner diameters 117 mm and 143 mm, respectively. Although the volume averaged field gradient for the MSS with the compensation coil of an inner diameter of 143 mm was already better than 5×10^{-4} cm^{-1} and was acceptable, it is expected that the field gradient for the MSS with non-identical compensation coils as shown in Fig. 1 would be even smaller. The simulation of the MSS with identical compensation coils gave a good indicator for the simulation of the CANDOR solenoid with non-identical compensation coils as the simulation for the MSS with non-identical compensation coils requires more complicated optimization of each individual compensation coil.

To optimize the field homogeneity of the CANDOR MSS with non-identical compensation coils, we began to tune the smaller compensation coil while fixing the larger compensation coil at 16 turns as determined from simulation with identical compensation coils. The optimal condition was determined to be 16 turns for the smaller compensation coil. The smaller compensation coil was then set to 16 turns and the procedure was repeated for the larger compensation coil. The optimal condition was determined to be 19 turns for the larger compensation coil. The volume averaged field gradient was calculated in every step. The above procedure was reiterated until the calculated volume averaged field gradient changed by less than 10^{-5} cm^{-1}. Fig. 2 shows an example of the calculated field B_{z} profiles by varying the number of turns of the smaller compensation coil while fixing the larger compensation coil to 19 turns. It appeared that 16 turns of the smaller compensation coil yielded the smallest volume averaged transverse field gradient.

Fig. 3 shows contour plots of the simulated B_{z} in the central plane (x=0). Shown in Fig. 3b is a contour plot zoomed from Fig. 3a centered around the most homogenous field region. The field in the center was about 2.73 mT and chosen to not saturate the mu-metal, provide a reasonably high field so that the effect from any external field to the field inside the MSS is minimal, and to achieve a very efficient AFP inversion of the ^{3}He polarization. The effect of compensation coils

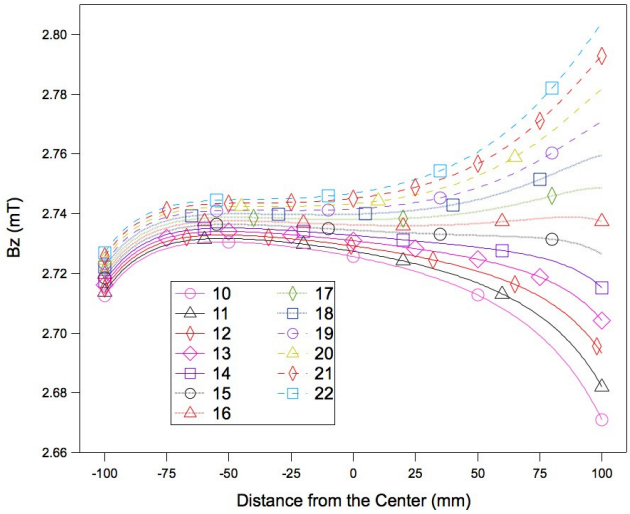

Figure 2. (Color online) Calculated B_z field profiles for different numbers of turns of compensation coils centered on the 117 mm diameter hole end cap with the compensation coil centered on the 143 mm diameter hole fixed to 19 turns. Lines are to guide the eye.

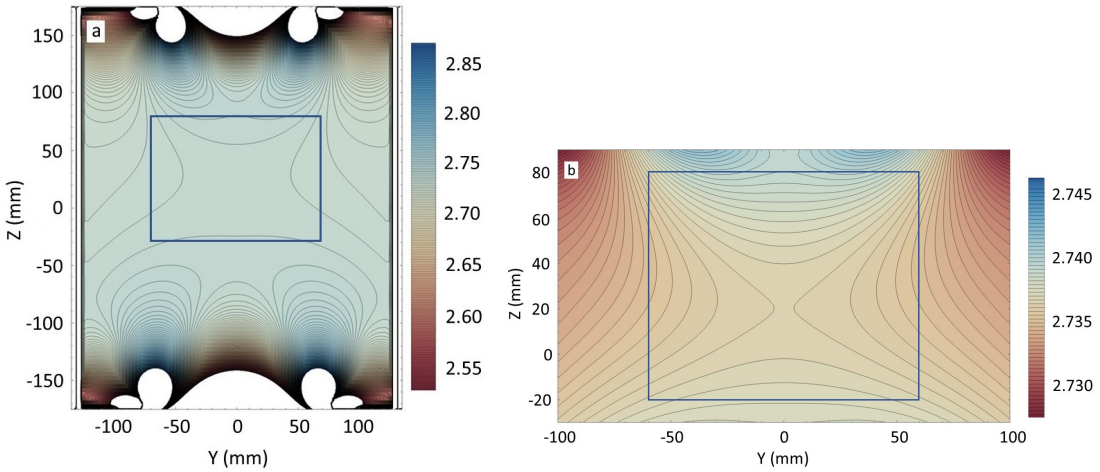

Figure 3. (Color online) Contour plots of the calculated B_z profile in the central plane (x=0) for the full size solenoid (a) and for the zoomed part centered around the most homogenous field region (b) at the optimized configuration of 16 turns and 19 turns of compensation windings attached to the small and large end cap hole, respectively. The field is in the unit of mT. The boxes in Fig. 3 indicates where the ^{3}He analyzer cell should be positioned.

was visible in Fig. 3a around the end cap holes and no magnetic flux saturation was observed near the main and compensation coils. The boxes in Fig. 3 represent a region with a minimal volume averaged field gradient and a region where the ^{3}He analyzer cell should be located. The field homogeneity center is shifted about 30 mm along z, as the center is expected at z=0 for a solenoid with identical compensation coils and holes in the end caps. In Fig. 3a, the two most inner magnetic flux lines represent a field difference of 2.2 μT, corresponding to a fractional field change $|\Delta B_z|/B$ of no worse than 8×10^{-4} over a cross sectional area of 150 mm by 120 mm. In Fig. 3b the two most inner flux lines represent a field difference of 0.27 μT, corresponding to a fractional field change $|\Delta B_z|/B$ of 1×10^{-4}. The region of good field homogeneity with $|\Delta B_z|/B \approx 1\times10^{-4}$ was about 70 mm along the z-axis and nearly 120 mm along the y-axis. We calculated the volume averaged field gradient $|\vec{\nabla}B_\perp/B|$ over the volume of a cylindrical ^{3}He cell, 120 mm diameter and 100 mm long, and obtained $|\vec{\nabla}B_\perp/B|\approx 3.5\times10^{-4}$ cm^{-1} at the optimized configuration with ampere-turn ratios of 0.059 between the smaller compensation coil and the main coil and 0.070 between the larger compensation coil and the main coil, respectively. This gradient was a factor of 1.37 smaller than that for the MSS with the identical larger compensation coils of a diameter of 143 mm, implying an improvement of a factor of 1.88 in the field gradient induced relaxation time. This improvement of the field gradient was obtained without sacrificing the scattering angle coverage. At the optimized condition, simulations yielded 16 turns and 19 turns of 16 AWG wire for the smaller and larger compensation coils, respectively.

After obtaining an improved field gradient, we explored more contour maps for the off-center regions along both x and z directions. It was observed that the calculated B_z field homogeneity is still good at x=60 mm that corresponds to the edge of the cell and is only slightly worse than that in the center. Fig. 4 shows contour plots of the calculated B_z profile along the radial direction at z=30 mm and at z=80 mm. In Fig. 4 (a) and (b), the two most inner flux lines represented a field difference of 0.27 μT, corresponding to a fractional field change $|\Delta B_z|/B$ of 1×10^{-4}.

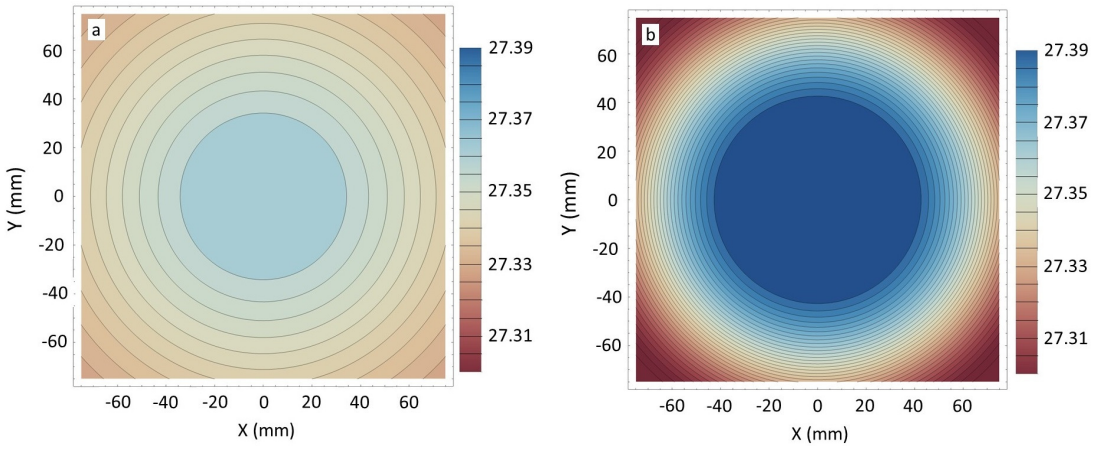

Figure 4. (Color online) Contour plots of the calculated B_z profile along the radial direction at z=30 mm (a) and at z=80 mm (b). The field is in the unit of mT.

3. Experimental results and discussion

We have designed and constructed a MSS based on modeling with the dimensions shown in Fig. 1. Each compensation coil was wound on an aluminum frame that was centered around

the hole of the corresponding end cap. Both the main and compensation coils used 16 AWG wire. The main coil consisted of 270 turns. A computer controlled mapping system was used for field mapping at different compensation coil conditions. A 3-axis Hall probe (Lakeshore 460 3-channel Gaussmeter with a HSE probe) and a 3-axis fluxgate magnetometer (Bartington MG-03MS) were used to measure the field. The fluxgate has a resolution of 1 nT and was used for measurements of magnetic fields lower than 1 mT. The hall probe has a resolution of 10 nT and was used for measurements of fields higher than 1 mT. The mapper could translate along both y and z directions. Many field maps were taken on the axis of the MSS with varying turns for both compensation coils as discussed in the modeling section. Fig. 5 shows an example of a set of measured B_z field profiles in the central plane x=0, which was in good agreement with the simulation. We measured the line averaged gradient along z over a 100 mm length centered at the most homogenous region for each field map and found that the line-averaged gradient $|\Delta B_z/\partial z|/B$ was minimized at 20 turns of compensation coils on the 143 mm diameter hole and 11 turns of compensation coils on the 117 mm diameter hole. At this configuration, the linearly averaged gradient was 9.3×10^{-5} cm^{-1}. Off-center axis field maps were also taken to check the field homogeneity at the different compensation coil configurations. The experimentally determined compensation coil configuration at the 143 mm end cap was in good agreement with the model. However it was 11 turns of compensation coil at the 117 mm end cap, somewhat deviated from the simulation. Any tiny air gap between the Conetic mu-metal cylinder and end cap occurring during fabrication would cause perturbation of the magnetic field, while no gap was assumed for the simulation. We have checked the effect of the air gap between the Conetic mu-metal cylinder and end cap for two conditions and found an air gap of 1 mm (0.5 mm) can change the optimized configuration for the smaller compensation coil from 16 turns with no air gap to 6 (10) turns. It was determined that an $\sim$ 0.35 mm air gap would be required to change the optimized smaller compensation coil from 16 turns to 11 turns. This would result in a nearly negligible change of the volume averaged gradient $|\vec{\nabla}B_\perp/B|$ (from 3.5×10^{-4} cm^{-1} to 3.6×10^{-4} cm^{-1}). In practice, each mu-metal end cap was designed to be snugly fitted onto the mu-metal cylinder body to allow for convenient and quick ^{3}He cell exchange (on the order of several seconds) to minimize ^{3}He polarization loss. It is likely that a tiny gap exists due to the fabrication process. We speculate this air gap is likely the main reason for the discrepancy between the experiment and simulation. However, other non-ideal geometric factors such as a small difference of compensation coil location, inhomogeneous permeability in the mu-metal, roundness of the mu-metal cylinder and end caps, and parallelism of the end cap might make additional contributions to the discrepancy.

After optimization of the CANDOR MSS, we measured the relaxation time of the CANDOR ^{3}He analyzer cell Sundown. Sundown has a diameter of 132 mm and a neutron path length of 92 mm, and is able to cover the scattering angle from the entire detector assembly. Sundown was filled to a partial ^{3}He pressure of 0.95 bar. We obtained a relaxation time of 690 h in a pair of large Helmholtz coils that yielded a field gradient $|\vec{\nabla}B_\perp/B|$ better than 1×10^{-4} cm^{-1}, corresponding to a field gradient induced relaxation time of about 14000 h [20]. The relaxation time measurement was done in the CANDOR MSS after optimization on the PHADES (Polarized ^{3}He And Detector Experiment Station) beam line at the NCNR. The ^{3}He polarization was determined using the neutron transmission method [24]. Fig. 6 shows the time-dependent ^{3}He polarization. The ^{3}He polarization decays exponentially with time and is given by $P_{\rm He}(t) = P^0_{\rm He} exp(-t/T_1)$, where $P^0_{\rm He}$ is the initial ^{3}He polarization. We obtained a ^{3}He polarization relaxation time of 414.6 h $\pm$ 2.4 h in Fig. 6. The extrapolated volume averaged field gradient $|\vec{\nabla}B_\perp/B|$ is $(3.7\pm0.2)\times10^{-4}$ cm^{-1}, in good agreement with that from the simulation. The initial ^{3}He polarization was 85 %. The final time averaged ^{3}He polarizations would 82.6 %, 80.3 %, and 78.0 % for experiments of 24 h, 48 h and 72 h duration, respectively.

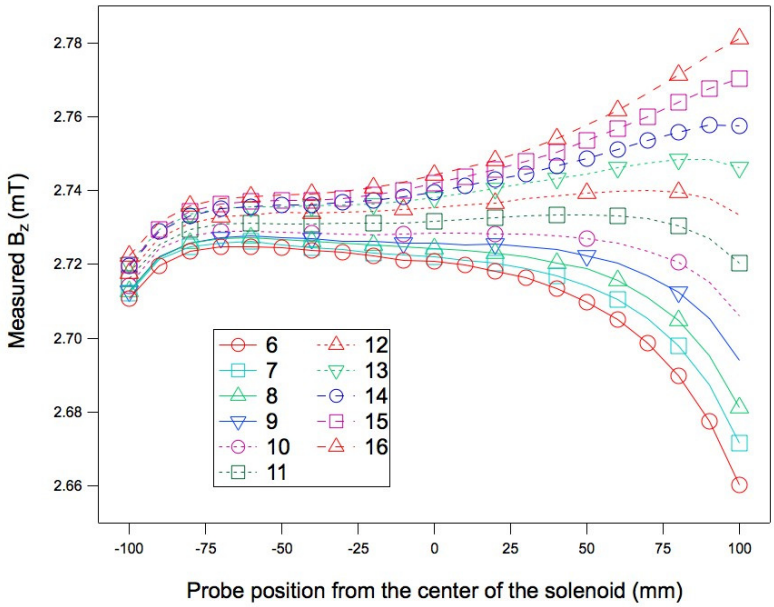

Figure 5. (Color online) Measured B_z field profiles for different numbers of turns of compensation coils centered on the 117 mm diameter hole end cap with the compensation coil centered on the 143 mm diameter hole fixed to 20 turns. The hall probe was used for these measurements. Lines are to guide the eye. Error bars are smaller than the data points.

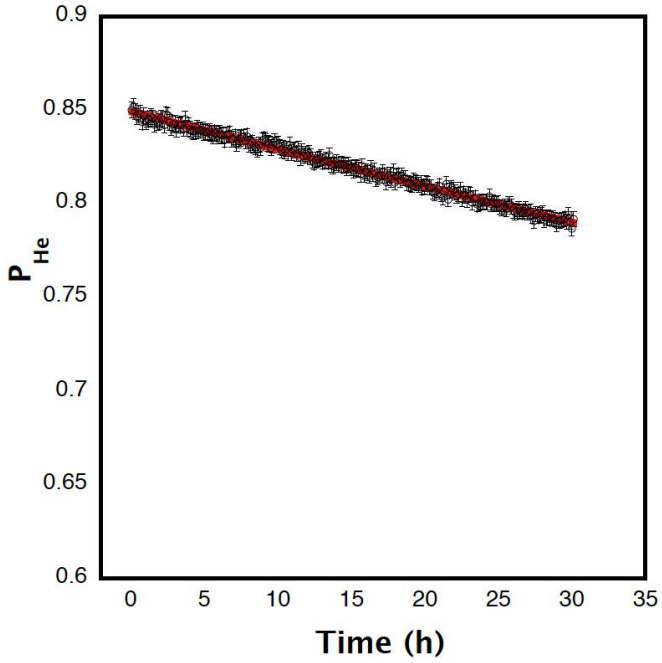

Figure 6. (Color online) The ^{3}He polarization P_{He} decay with time for the cell Sundown that will be used on CANDOR after optimization of the CANDOR MSS. The red solid line is the best fit to an exponential decay of ^{3}He polarization, yielding a relaxation time T_1 of 414.6 h $\pm$ 2.4 h. Error bars and uncertainties represent one standard deviation.

4. Conclusions

We have simulated and optimized the magnetic field gradients of a magnetically shielded solenoid (MSS) for the ^{3}He neutron spin filter that will be used as a spin analyzer on the new polychromatic reflectometer CANDOR at the NCNR. We have calculated the volume-averaged transverse field gradient which is directly linked to the field gradient-induced ^{3}He polarization relaxation time. Based on the simulation, we have constructed and characterized a compact MSS that has a dimension of 279 mm in diameter and 356 mm long. The MSS has a Conetic mu-metal cylindrical solenoid with an end cap attached to either end. By applying non-identical compensation coils centered to the hole on each end cap, we have found that the center where the field is most homogenous shifted ≈30 mm closer to the end with a smaller compensation coil. Hence the ^{3}He analyzer cell should be placed closer to the sample, which allows its diameter to be reduced. We have also shown that the volume-averaged field gradient over the cell was reduced by a factor of 1.37, hence the field gradient induced relaxation time was improved by a factor of 1.88 compared to that with identical compensation coils. We have obtained a ^{3}He polarization relaxation time of 414.6 h ± 2.4 h for a ^{3}He cell 132 mm in diameter and 92 mm long after optimization of the CANDOR MSS. After correction to the intrinsic relaxation time of 690 h, the volume averaged field gradient was determined to be $(3.7\pm0.2)\times10^{-4}$ cm^{-1}, agreeing well with the calculation (3.5×10^{-4} cm^{-1}). In the near future, we will develop a ^{3}He adiabatic fast passage NMR flipper that is integrated into the ^{3}He analyzer. We plan to characterize the overall polarization analysis capability as soon as CANDOR is available.

Acknowledgments

We thank Jeff Anderson and Jack Fuller of the NIST glassblowing and optical shops. We thank Ross Erwin for his help with the RADIA simulation software and Shannon Watson for her help with construction of the magnetic shielded solenoid. Discussions with Thomas Gentile are gratefully acknowledged. The work utilized facilities supported in part by the National Science Foundation under Agreement No. DMR-1508249.

References

[1] https:/ /ncnr.nist.gov/equipment/msnew/ncnr/candor.html
[2] Groitl, F *et al.*, 2017 *Sci. Rep* **7** 13637
[3] Osovizky, A *et al.*, 2018 *J. Phys. Commun.* **2(4)**, 045009.
[4] SwissNeutronics AG, Bruehlstrasse 28, CH-5313 Klingnau, Switzerland. Certain trade names and company products are mentioned in the text or identified in an illustration in order to adequately specify the experimental procedure and equipment used. In no case does such identification imply recommendation or endorsement by the National Institute of Standards and Technology, nor does it imply that the products are necessarily the best available for the stated purpose.
[5] A special RF flipper has been developed to flip the incident neutron spin with a flipping efficiency better than 0.999 for the entire 6 cm by 15 cm beam. The results will be published elsewhere.
[6] Abragam A 1961 *The Principles of Nuclear Magnetism* Oxford University Press, Oxford, England
[7] Chen WC *et al.* 2014 *Journal of Physics: Conference Series* **528** 012014
[8] Chen WC *et al* 2003 *Physica B* **335** 196
[9] Chen WC, Gentile TR, O'Donovan KV, Borchers JA, Majkrzak CF 2004 *Rev. Sci. Instrum.* **75** 3256
[10] N.R. Newbury *et al.*, 1993 *Phys. Rev. A* **48** 4411
[11] W.A. Fitzsimmons, L.L. Tankersley, and G.K. Walters, 1968 *Phys. Rev.* **179** 156
[12] L.D. Schearer and G.K. Walters, 1965 *Phys. Rev.* **139**, A1398-A1402
[13] Chen WC *et al.* 2014 *J. Appl. Phys.* **116** 014903
[14] Chen WC *et al.* 2011 *Journal of Physics: Conference Series* **294** 012003, and references therein
[15] Salhi Z, Babcock E, Pistel P, and Ioffe A 2014 *Journal of Physics: Conference Series* **528** 012015
[16] Gentile TR *et al* 2005 *Physica B* **356** 96
[17] Chen WC *et al* 2007 *Physica B* **397** 168
[18] Chen WC *et al* 2009 *Physica B* **404** 2663

[19] Magnetic Shield Corporation, 740 N. Thomas Drive, Bensenville IL 60106. Co–Netic mu-metal has a higher magnetic permeability than that of Netic mu-metal.
[20] McIver J W, Erwin R, Chen W C and Gentile T R 2009 *Rev. Sci. Instrum.* **80** 063905
[21] Cates G D, Schaefer S R and Happer W 1988 *Phys. Rev. A* **37** 2877
[22] Chubar O *et al.*, Proceedings of EPAC 2004, Lucerne, Switzerland, p. 1675.
[23] http:/ /www.wolfram.com/mathematica/.
[24] Jones G L *et al.* 2000 *Nucl. Instrum. Meth. A* **440** 772